ON THE AERODYNAMIC INSTABILITY IN A SWIRL COMBUSTOR OPERATING WITH LEAN PREMIXED HYDROGEN-ENRICHED METHANE BLEND

S. Qiu, E. Karlis, A. M. K. P. Taylor and Y. Hardalupas
s.qiu20@imperial.ac.uk
Department of Mechanical Engineering, Imperial College London,
Exhibition Road, SW7 2AZ, UK

Abstract
It is important to be able to understand and control the transition to strong thermoacoustic oscillation associated with the swirl combustor of, *e.g.*, gas turbines. We focus on the contribution of aerodynamic instability to the onset of thermoacoustic oscillation on a 33kW swirl stabilized combustor operating with lean premixed H_2-enriched CH_4 blend. Global CH* chemiluminescence and dynamic pressure shows that the combustion transits from a quiescent to a limit-cycle state as the H_2 molar concentration increases from 20% to 40%. The global (CH_4 and H_2) equivalence ratio was kept at 0.55 and the thermal heat release was almost constant at 33kW. Linear stability analysis is applied to solve the linear perturbation mode of the non-reacting swirling jet, and shows the existence of a dominant, helical mode perturbation and a secondary, center mode perturbation. This is confirmed experimentally by using proper orthogonal decomposition (POD) and dynamic mode decomposition (DMD) to extract coherent flow structure from time-resolved PIV snapshots of both non-reactive and reactive flow. It is found that the helical mode gives rise to the precessing vortex core (PVC) by inducing a sequence of downstream propagating vortical perturbations. The helical mode and its induced PVC motion is found to *diminish* as the system transits from quiescent state to a limit-cycle oscillation. In the transitioning case, a streak-structure perturbation, which resembles the center mode, becomes *dominant*. The center mode is distinguished from the helical mode in that it is localized near the centerline of the swirl and is marginally stable under non-reacting condition. It is inferred from the present research that the PVC motion is not the only coherent flow structure that the flame interacts with to trigger thermoacoustic oscillation; the center mode may play a role in the triggering event, which needs further investigation.

1. Introduction
Thermoacoustic oscillation is an oscillation of pressure and heat release rate that occurs when the unsteady heat release rate is in phase with acoustic fluctuation. In industry, the issue of thermoacoustic oscillation arises as a side-effect of the application of lean-combustion technology. This technology aims to reduce the emission of thermal NOx and particulates; it has been increasingly applied to airborne or land-based gas turbine combustor [1]. However, this mode of combustion is found to be susceptible to the triggering of thermoacoustic oscillation. The oscillation arises in a self-excited and very often abrupt manner as the operation parameter of the combustor changes. The associated dynamic loading and enhanced heat transfer limit the operation range of the combustor, leading to a deterioration in system performance or even causing structural damage to the combustor [2].

Despite the effort that has been put into alleviating this problem, the challenge remains because when, and why, thermoacoustic oscillation arises is difficult to predict. This is due to the multi-physics nature underlying thermoacoustic oscillation, which associates combustion, acoustics and aerodynamics instability. Research shows that thermoacoustic oscillation in swirl-stabilized combustor of gas turbine engine is related with an interaction between a

coherent flow structure induced by an aerodynamic instability, known as the precessing vortex core (PVC), and the flame's structure [3]. However, it is still ambiguous as to how the onset of PVC in stabilized combustors relates to the transition from a quiescent state to thermoacoustic oscillation. It has been reported that the PVC induces a 'lower stagnation point' [4] that causes the lift-off of the flame; the lifted flame then further amplifies the aerodynamic instability. In several other studies, it was argued that it is the change of operation condition, e.g., the equivalence ratio, that modifies the flame shape from V-shape to M-shape. The change of flame structure either excites or suppresses the PVC, and further leads to the onset or decay of thermoacoustic oscillation [5][6][7]. In some scenarios, however, it was found that the PVC was *suppressed* during combustion [8][9][10].

The understanding of the transition mechanism is important for the prediction of the occurrence of thermoacoustic oscillation. Kim and Hochgreb [11] identified six distinct stages in triggering during the temporal evolution of a model gas turbine combustor. From an initial small perturbation, the system goes through an exponential growth, followed by saturation due to nonlinearity, and then evolution towards a new stable periodic solution until a limit cycle is established. The transition from a quiescent case to a limit cycle can be achieved by a transient growth mechanism. The combination of linear perturbations can undergo a transient growth in the short term, even though each linear perturbation decays in the long term. This is because of the non-normality of the system operator [12]. For a Rijke tube, the gain of the transient growth can be 10; for a more complex geometry, e.g., a real gas turbine combustor, this gain can be up to 10^6 [13]. Consequently, a noise-level perturbation may trigger the system and cause drastic shift in the system state. The transient growth mechanism prevails especially in the scenario of a subcritical Hopf bifurcation [14]. In this scenario, both the quiescent state and limit-cycle state are a stable solution of the system. The transient growth of perturbations can be large enough to cause the system to deviate from the quiescent solution and be captured by the limit cycle 'attractor'.

In the present research, we investigate the dynamics of a small scale ($33kW_{th}$) model gas turbine combustor operating with a lean premixed hydrogen-enriched methane fuel supply. The hydrogen addition improves the methane by increasing flame speed and flame temperature, and it alters the thermoacoustic state of the combustion. As the molar concentration of hydrogen in the fuel blend increased from 20% to 40% while the global (CH_4 and H_2) equivalence ratio was kept constant at 0.55, the system transited from a quiescent state to an intermittent state, and then into limit cycle. Despite the previous research on the interaction of PVC and flame structure as well as on the transition through a transient growth mechanism, it is still unclear what triggers the system into thermoacoustic oscillation. In the present research, we aim to understand the contribution of aerodynamic instability to the onset of thermoacoustic oscillation for the hydrogen-enriched methane fuel. Linear stability analysis is applied to the non-reacting flow to solve the linear perturbation modes, and mode decomposition techniques extract coherent flow structures from the PIV snapshots of both non-reacting and reacting flow.

2. Method

2.1 Experimental technique

The experiment was conducted on small scale ($33\ kW_{th}$) model gas turbine combustor. A sketch of the combustor rig is shown in Figure 1 and can also be referred to in [15]. The air was supplied at 4 barg. The fuel blend was injected after the swirler, out of 10 equidistant, radially positioned holes on the centrebody. A 100mm distance between the injection point and the diffuser allowed adequate premixing of fuel and air [16]. After the centrebody, a diffuser allowed a recirculating flow to be established in the fused silica tube. The diffuser distinguishes our rig from many with a step area expansion following the centrebody, where an outer

recirculation zone is produced. Optical measurements were made through the fused silica tube to measure the unsteady flow field and flame structure.

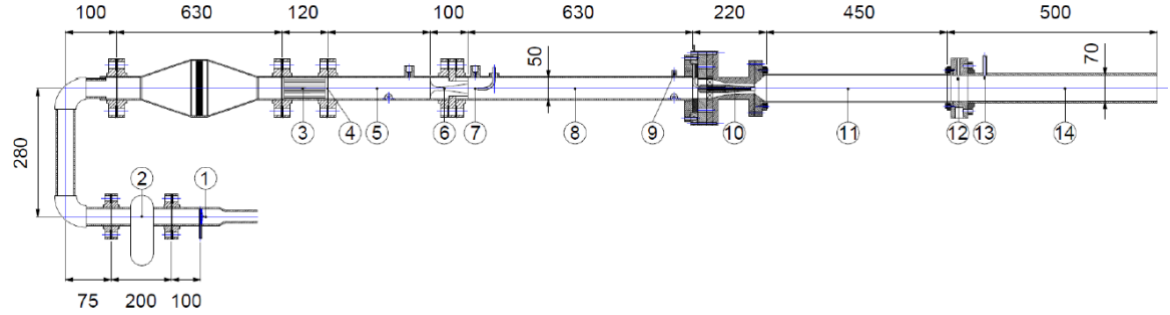


Figure 1. Sketch of the swirl combustor rig. 1: upstream counterflow fuel injector for fully premixed measurement; 2: pressure reducing valve; 3: tube bundle flow straightener; 4: wire mesh gauge; 5: flow preconditioner; 6: critical Venturi nozzle; 7: seeding nozzle; 8: inlet plenum; 9: upstream dynamic pressure tapping; 10: swirler; 11: fused silica combustor; 12: spark plug igniter; 13: semi-infinite tube tapping; 14: exhaust. Dimensions are in mm.

High speed particle image velocimetry (PIV) was applied to temporally resolve the unsteady jet produced by the swirler. The seeding particles were illuminated by a 532nm Nd: YAG laser @3kHz. The field of view was 60×60mm2. The resolution of the processed PIV vector field was 0.47mm. The dynamic pressure in the combustor was measured as an indicator of thermoacoustic state. The dynamic pressure was sampled at 20kHz by a microphone (Kulite MIC-190M) installed to a semi-infinite tube at the exhaust. The purpose of the semi-infinite tube is to prevent any interference of the measurement with the acoustic field. In addition, the global CH* chemiluminescence intensity was acquired as an indicator of heat release rate. It was acquired at 20kHz by a photomultiplier as described in [17].

2.2 Linear stability analysis

Linear stability analysis (LSA) was performed upon the non-reacting flow field to solve the temporal/spatial evolution of small perturbations numerically. The instantaneous flow field in cylindrical polar coordinates $\mathbf{q} = [u_r, u_\theta, u_z, p]$ is decomposed into a steady base flow $\overline{\mathbf{q}}$ and a small perturbation $\mathbf{q}'$. The perturbation is then spanned into a Fourier series $\mathbf{q}'(\tilde{r}, \theta, \tilde{z}, \tilde{t}) = \hat{\mathbf{q}}(\tilde{r})\exp(i\varphi)$. The tilde denotes non-dimensional variables, where the reference length is the inner radius R of the fused silica tube and reference velocity is the bulk velocity U_{bulk}. The phase φ is a function of the nondimensional coordinates $(\theta, \tilde{z}, \tilde{t})$, whereas $\hat{\mathbf{q}}(\tilde{r}) = [\hat{u}_r, \hat{u}_\theta, \hat{u}_z, \hat{p}]$ is the mode shape. The small perturbation is obtained by solving the generalized eigenvalue problem $\mathbf{A}\hat{\mathbf{q}} = \omega\mathbf{B}\hat{\mathbf{q}}$ rearranged from the linearized Navier-Stokes equation, where ω is the complex frequency of the perturbation. Details for the operator **A** and **B** are found in [18][19].

2.3 Mode decomposition technique

Two mode decomposition techniques were applied to the PIV snapshots of both reacting and non-reacting flow, the Proper Orthogonal Decomposition (POD) and the Dynamic Mode Decomposition (DMD). The POD analysis extracts the dominant coherent flow structures, which are sorted by the kinetic energy they contain. In POD analysis, the PIV snapshots are spanned by $u(\boldsymbol{x}, t_k) \approx \sum_{p=1}^{N} a_p(t_k)\Phi_p(\boldsymbol{x})$, where $a_p(t_k)$ is the temporal coefficient, $\Phi_p(\boldsymbol{x})$ is the spatial POD mode[20], and $\boldsymbol{x}$ is the coordinate vector; p and k is the index of POD mode and discrete time t.

DMD analysis was applied to decompose the PIV snapshots into coherent spatial modes in terms of their frequencies. The advantage of DMD is to reconstruct the system dynamics with

solely the measurement, without the knowledge of the system matrix. The timeseries of the snapshots is reconstructed by $u(t) \approx \sum_{s=1}^{r} \phi_s \exp(\omega_s t) b_s$, where ϕ is the DMD mode, ω is the complex frequency and b is the initial amplitude of each mode; s is the index of DMD mode and r is the truncation rank. Details of the DMD algorithm can be found in [21][22].

3. Aerodynamic instability of the non-reacting swirling jet

The combustor produces a confined swirling jet, as shown in Figure 2(a). The Reynolds number based on the U_{bulk} and R is 13000, with the density and viscosity of the cold flow being 1.2kg/m^3 and 1.8e-5kg/(m·s), respectively. The flow expands in the diffuser and, due to the adverse pressure gradient, a recirculation zone is produced. Figure 2(b) shows the time-averaged tangential and streamwise velocity profile. The tangential velocity profile was fitted to a modified Burgers vortex[23], and the axial velocity was fitted to a Gaussian profile before they were taken as the base flow in stability analysis. This procedure ensures that the base flow is an exact solution to the Navier-Stokes equation and filters out the noise in experiment[24], preventing spurious solutions in the stability analysis.

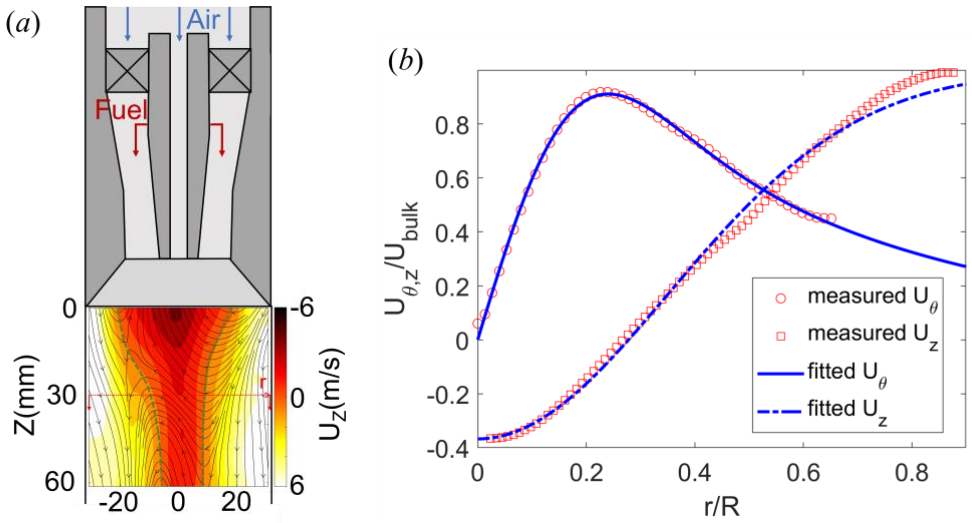


Figure 2. (a) Time averaged flow field of the isothermal swirling jet. Green dashed line shows the boundary of recirculation zone (defined as the locus of the axial component of velocity $U_z = 0$). (b) Tangential and axial velocity profiles. The tangential velocity is measured from the cross-sectional plane at z=30mm.

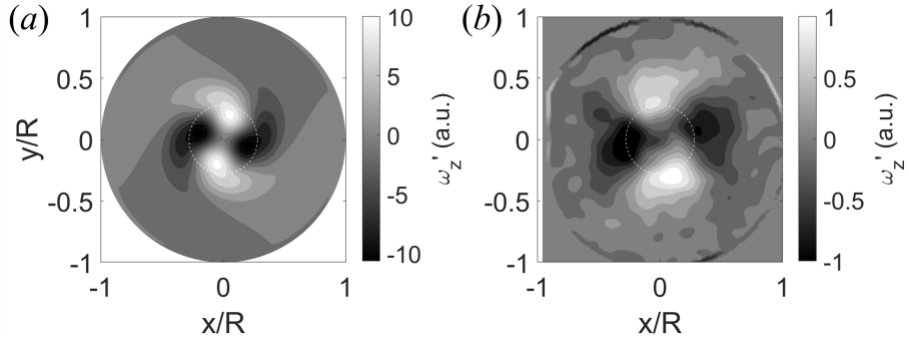


Figure 3. (a) The dominant linear perturbation mode with azimuthal wavenumber of 2 of the non-reacting swirling jet; (b) the most energetic POD mode (2nd mode) extracted from cross-sectional measurement in non-reacting flow. The contour shows the axial component of the vorticity perturbation (ω_z'). The dotted circle denotes where U_z = 0.

Figure 3(*a*) shows the dominant linear perturbation mode calculated from the stability analysis. The dominant mode shows a 'double-helix-like' shape in the axial vorticity contour, which winds around the recirculation zone, here taken to mean where $U_z = 0$. The dominant linear perturbation mode is compared to the most energetic POD mode as shown in Figure 3(*b*). The POD mode shows something which has some measure of resemblance to the double-helix structure.

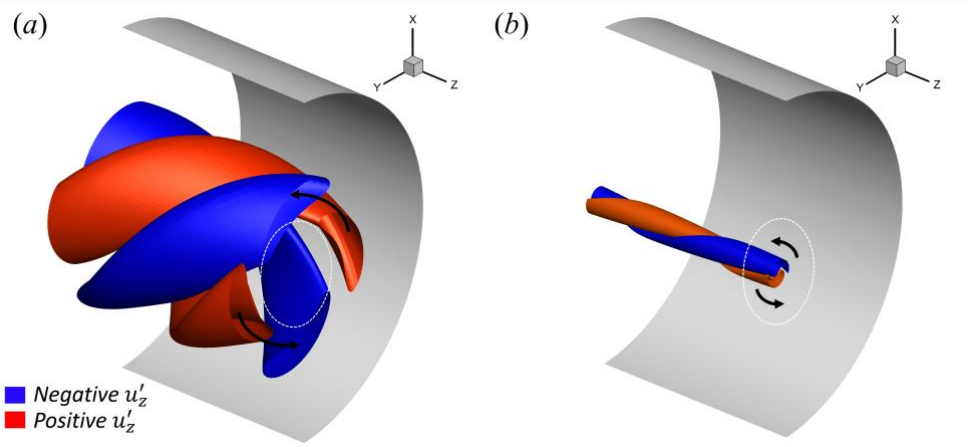


Figure 4. Three-dimensional structure of the linear stability mode: (*a*) the dominant, helical mode for axial velocity perturbation; (*b*) the secondary, center mode. The iso-surface and contour show the axial velocity perturbation. The gray surface denotes the location of the fused silica tube; the circle denotes the extent of the recirculation zone. The *z*-range of the center mode is scaled to the wavelength of the dominant mode in this figure.

The linear stability analysis revealed two linear perturbation modes, the dominant, helical mode and the secondary, center mode. Their three-dimensional structure is shown in Figure 4. The dominant perturbation mode shows a helical structure at the periphery of the recirculation zone It is unstable as derived from the stability analysis, with an axial wavelength of 4cm and frequency of 110Hz. The secondary, center mode, on the other hand, is marginally stable. It also shows a helical structure but localized near the centerline of the swirl. The axial wavelength of the center mode is 55cm and its frequency is 152Hz. Both modes are counter-handed to the direction of the swirl, but both rotate in the same direction as the swirl.

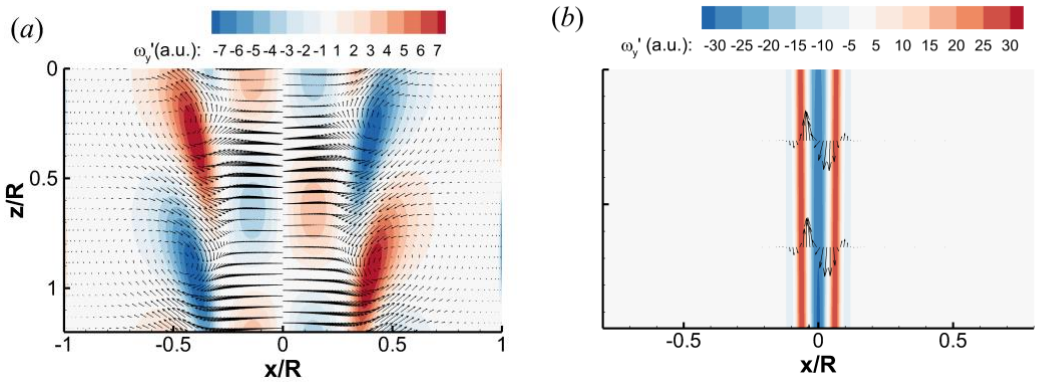


Figure 5. An axial-radial slice of (*a*) the dominant, helical mode, and (*b*) the secondary, center mode. The vectors show the in-plane velocity perturbation. The range of *x*-coordinate in (*b*) is set to match with that in Figure 7(*b*).

Figure 5 shows how the two modes perturb the swirling jet. Figure 5(*a*) shows that as the dominant, helical mode travels downstream, it induces a velocity perturbation which undulates locally with time. The undulating velocity perturbation generates a sequence of vortices which

perturb the flow periodically as they travel downstream. The secondary, center mode as in Figure 5(*b*) also induces an undulating velocity perturbation. However, the perturbation is close to the centerline of the swirl, showing a streak-like pattern. This mode is stable, possibly because of the restoring effect of the Coriolis force inside rigid body rotation [25].

4. Dynamics of thermoacoustic oscillation

In this study, the swirl combustor was operated with three H_2 molar concentrations in the CH_4 blend, as shown in Table 1. The equivalence ratio was kept to 0.55±0.01 and the thermal power was constant to better than 3%. A pressure transducer in the fuel line upstream the injection point confirmed that the fuel mass flow rate was not oscillating in sympathy with thermoacoustic instability [26]. At this equivalence ratio, the combustor transits from quiescent combustion to a limit-cycle oscillation as χ_{H2} increases from 20% to 40%. The bulk flow within the combustor accelerates under the reactive condition, yielding a Reynolds number of 19000.

Table 1. Experimental operation conditions

[χ_{CH4}, χ_{H2}]	Φ	Dynamic state	P_{th} (kW)
[80%, 20%]	0.55	Quiescent	33.10
[70%, 30%]	0.55	Intermittent	33.47
[60%, 40%]	0.55	Limit cycle	33.91

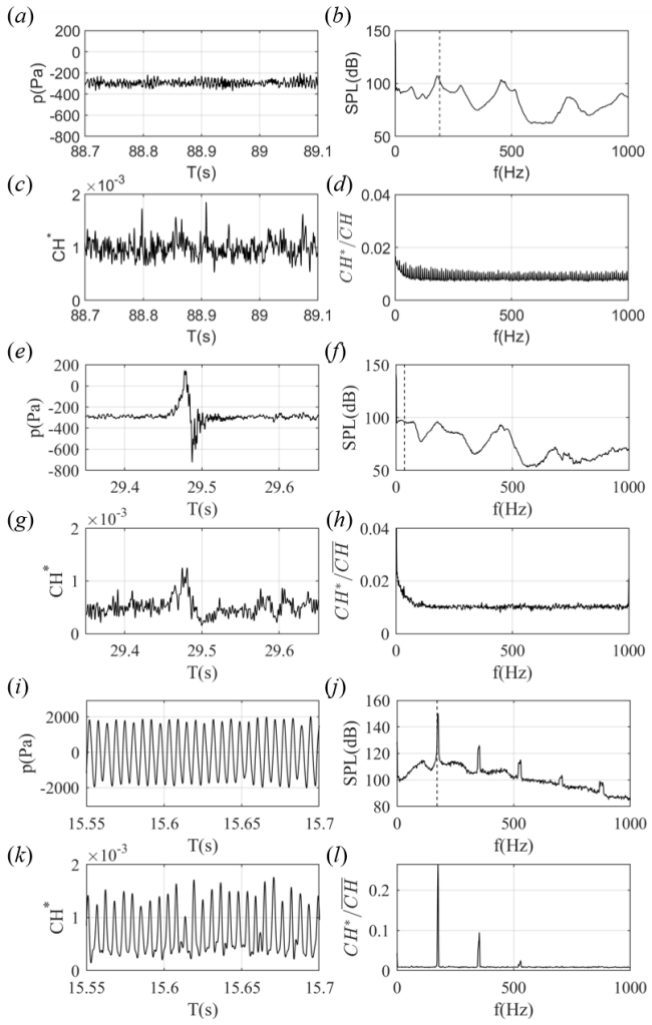


Figure 6. Time series (left column) and Fourier spectra (right column) of the dynamic pressure and global chemiluminescence CH* intensity for the quiescent case (*a*-*d*),

intermittent case (*e-h*), and limit-cycle case (*i-l*). The dashed line shows the frequency peak of the most energetic POD mode (Mode 2).

4.1 Frequency domain characteristics

The measured time series and frequency domain characteristics of the dynamic pressure and global CH* signal in the combustor is shown in Figure 6. For the quiescent case as in Figure 6(*a-d*), no significant periodical oscillation is observed in either the dynamic pressure or the CH* signal. Only a mild frequency peak at 180Hz is found in the frequency domain of dynamic pressure. No frequency peaks can be seen in the CH* frequency domain, which corroborates that the combustion was quiescent. For the intermittent case, as in Figure 6(*e-h*), a sudden burst of pressure occurs at the same time as an abrupt change in heat release rate, as shown in the time series of the dynamic pressure and CH* signal. This is a precursor indicating that the system is transiting into an oscillation, but no significant frequency peaks are found either in the dynamic pressure or CH* signal in this case. For the limit-cycle case as in Figure 6(*e-h*), the dynamic pressure and CH* intensity both oscillate with a large amplitude, and a clear frequency peak locates at 176Hz with a few harmonics for both signals. This shows that the system has entered a perpetuating thermoacoustic oscillation.

4.2. Coherent structures

4.2.1. The most energetic POD modes

To characterize the aerodynamic instability of the swirl jet in these distinct thermoacoustic states, the most energetic POD modes are extracted to show the dominating coherent flow structure for each case, as shown in Figure 7.

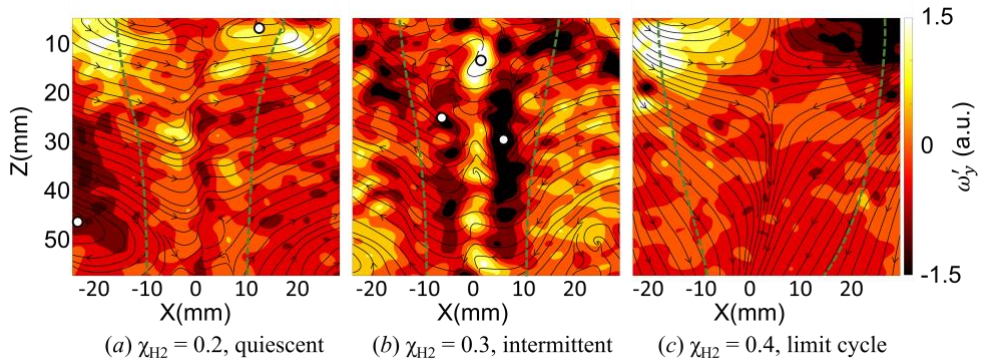


Figure 7. The most energetic POD mode for (*a*) the quiescent case, (*b*) the intermittent case, and (*c*) the limit cycle case. Flow is from top to bottom in each plot. The white dots show the location of the vortical flow; green dashed line shows the boundary of the recirculation zone (defined as the locus of the axial component of velocity $U_z = 0$).

For the quiescent case, the most energetic POD mode shows vortical flows at the periphery of the recirculation zone. This vortical flow around the recirculation zone is qualitatively similar to the result from the stability analysis (Figure 5(*a*)). The dominating frequency in the Fourier spectrum of its POD time coefficient is 190Hz, which is close to the frequency peak in the pressure and CH* signal (Figure 6(*b*)). For the intermittent case, the most energetic POD mode shows an elongated, streak-like vortical perturbation near the centerline of the swirling jet. Notably, this streak-like mode is wider in diameter but similar in shape and location to that of the secondary, center mode as in Figure 5(*b*). For the limit-cycle case, the most energetic POD mode becomes a 'pumping' mode, which periodically compresses and stretches the swirling jet; this motion will be further considered in the next section in connection with fig. 13. Fourier spectrum of POD time coefficients shows that the dominating frequency of this mode is 172Hz, which is identical to the frequency peak in the pressure and CH* signal (Figure 6(*j*)). This

indicates that this mode is one driving force that perpetuates the oscillation. In addition, the vortical structures become visible after the 13th mode only, which indicates that the vortical structures are suppressed in this case.

4.2.2. The DMD modes

To further capture the dynamics of the coherent flow structure for each case, DMD analysis was applied to the PIV snapshots. In each case, 1000 snapshots were used in the DMD analysis to ensure that at least 15 periods of the mode of interest were included. A truncation rank of 600, which contains at least 85% of the total energy, was then applied to discard high dimensional basis. Each extracted mode in this section correspond to the mode with the largest coherent measure[21], apart from the steady mode, in each measurement.

Figure 8 shows the DMD mode at f = 160Hz extracted from the cross-sectional measurement of the non-reacting swirling jet. The DMD mode has some resemblance to the dominant linear perturbation mode (Figure 3(*a*)), both showing traces of a double-helix structure, co-rotating with the swirl. This indicates that this DMD mode extracted from the measurement is probably associated with the helical mode from the aerodynamic instability of the swirling jet. The reconstructed dynamics using this DMD mode shows a precessing motion of the vortex, as shown in a cartoon linked here. Figure 9 further shows the reconstructed dynamics from the DMD mode at f = 172Hz in the axial-radial plane. The proximity of its frequency with that of the mode in Figure 8 implies that the two modes correspond to the same coherent structure. It can be observed that the recirculation zone of the swirling jet is flapping about its centerline in a periodical manner. We believe that this motion exhibits a sign of PVC, and it corroborates that PVC is driven by the dominating perturbation mode of the swirling jet, i.e., the helical mode.

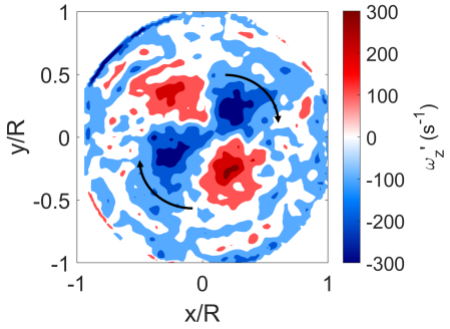


Figure 8. The DMD mode at f = 160Hz of the non-reacting swirling jet. The arrows denote the rotation of the mode. A cartoon showing the reconstructed dynamics using this DMD mode is linked here.

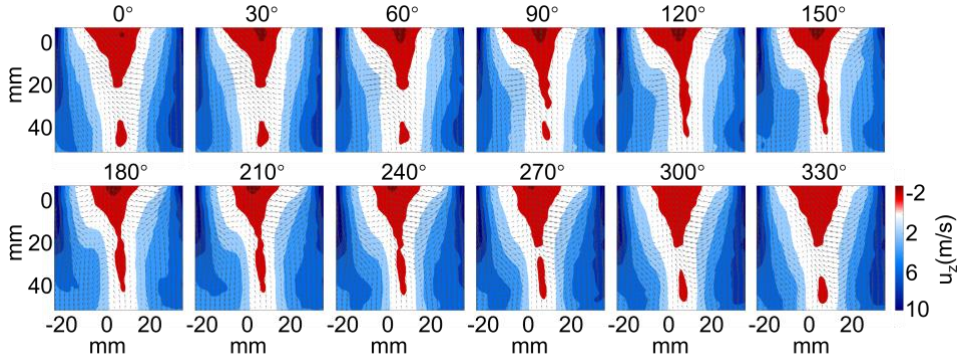


Figure 9. The dynamics reconstructed with the DMD mode at f = 172Hz of the isothermal swirling jet in the axial-radial plane.

The top panel of Figure 10 shows the DMD mode at f = 203Hz extracted from the quiescent case; it is then compared to the most energetic POD mode (also shown in Figure 7(*b*)). The purpose is to show that the two modes represent the same coherent structure. It can be observed in the left and middle panel that the transverse and streamwise velocity show similar distributions. The vorticity contour also shows similar pattern, where vortical flows around recirculation zone transport downstream. Moreover, the frequency of both modes is close to the frequency peak in Figure 6(*b*). The deviation between the two frequencies can be because the POD mode also contains other frequencies components, while the DMD mode is purely coherent. Therefore, it should be safe to say that the most energetic mode of the quiescent case is captured by its DMD mode at f = 203Hz.

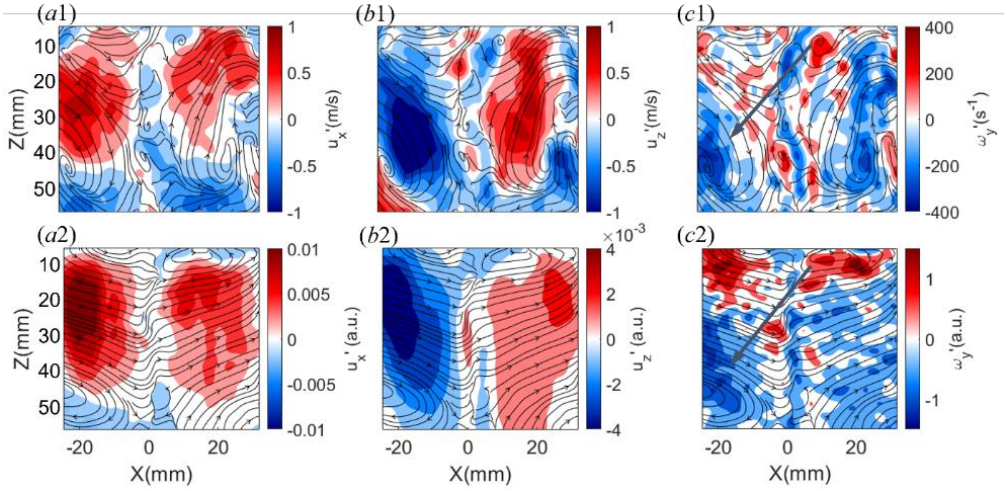


Figure 10. Comparison between the DMD mode at f = 203Hz (*a*1)(*b*1)(*c*1) and the most energetic POD mode (*a*2)(*b*2)(*c*2), both for the quiescent case.

The DMD mode at f = 203Hz is then used to reconstruct the dynamics of the quiescent case, as shown in Figure 11. It shows that the precessing motion persists for the quiescent case, where the recirculation zone precesses periodically. It is also observed that the recirculation zone occurs further downstream compared to the isothermal case. It can be inferred here that the precessing motion does not trigger the thermoacoustic oscillation by itself, as the combustion is quiescent in this case. In terms of triggering oscillation, the complex interaction between the flame and the unsteady flow should be considered as in, e.g., [4][7].

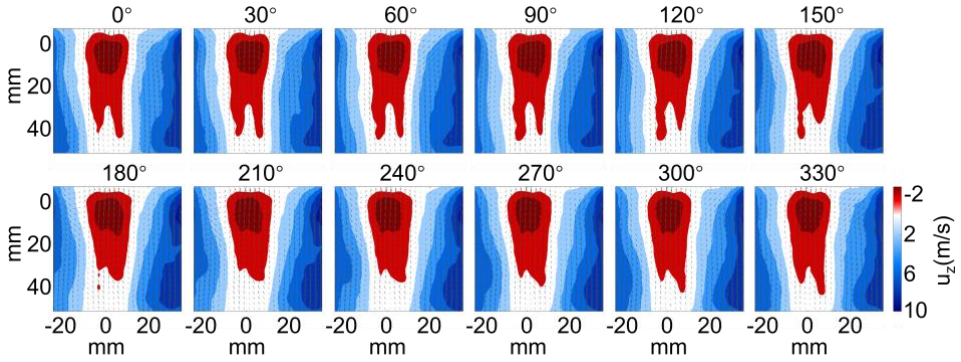


Figure 11. Dynamics reconstructed with the DMD mode at f = 203Hz of the quiescent case.

Figure 12 shows the DMD mode at f = 63Hz for the intermittent case, which is the mode with the largest coherent measure except for the steady mode. This DMD mode reproduces the streak-like perturbation as shown in the centre mode (Figure 5(*b*)) from the stability analysis and the most energetic POD mode (Figure 7(*b*)). The temporal evolution of this DMD mode in Figure 12 shows that the perturbation rotates as it propagates downstream; this is also identical

to the propagation of the centre mode. The resemblance between these two modes indicates that the centre mode, otherwise stable under the isothermal condition, dominates in the intermittent case. It is possible that the centre mode is amplified through transient growth by combining with another mode. More attention will be focused on the dominance of the centre mode in the intermittent case in future work.

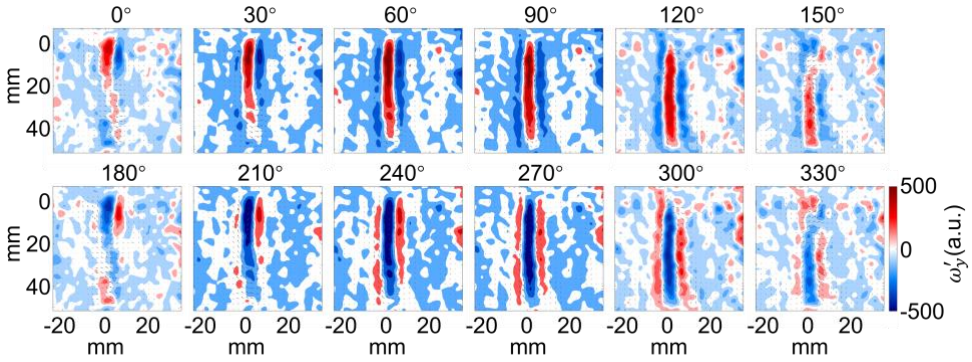


Figure 12. The DMD mode at f = 63Hz of the intermittent case.

The dynamics reconstructed with the DMD mode at f = 176Hz of the limit-cycle case is shown in Figure 13. The axial pulsation of the recirculation zone is clearly captured. It shows that the fundamental frequency at f = 176Hz is indeed associated with the 'pumping' motion of the recirculation zone. The subharmonic at $f \approx$ 120Hz and 1st harmonic at f = 352Hz were also examined but these two modes are not shown here for brevity. The subharmonic mode manifests itself as a low amplitude, precessing motion superimposed on a pumping motion, while the 1st harmonic mode exhibits an undulating motion superimposed on a pumping motion.

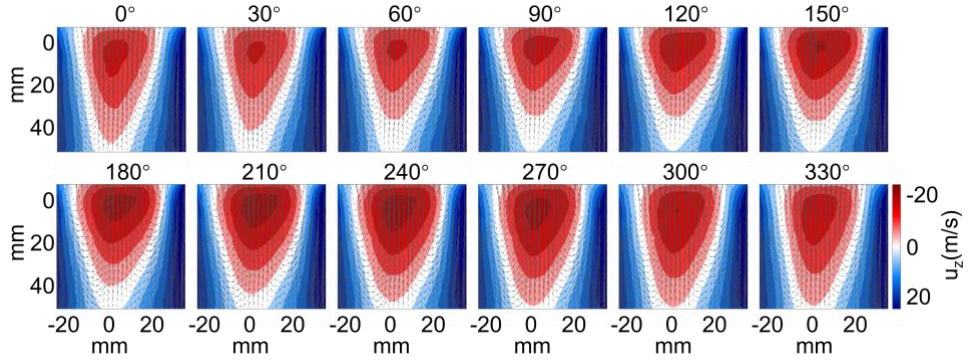


Figure 13. Dynamics reconstructed with the DMD mode at f = 176Hz of the limit-cycle case.

5. Discussion & Conclusion

We have focused on the contribution of aerodynamic instability to the onset of thermoacoustic instability on a swirl combustor rig operating with lean premixed hydrogen methane blend. Time-resolved measurements of velocity field, global CH* chemiluminescence and dynamic pressure characterized the unsteady flow field of the swirling jet and the thermoacoustic state of the combustor. Experimental results show that the combustor transits from quiescent state to a limit-cycle state as the molar concentration of hydrogen increased from 20% to 40%. Linear stability analysis was applied to solve the linear perturbation mode of the non-reacting swirling jet, and POD and DMD extracted coherent structures from the PIV snapshots of both the non-reacting and reacting flow. It is found that two linear perturbation modes exist in the swirling jet: a dominant, helical mode and a weaker secondary, center mode. The dominant, helical mode gave rise to the PVC by inducing a sequence of vortical perturbations propagating downstream. The helical mode dominates in the isothermal condition, but in reacting flow its importance

diminishes as the combustion goes from quiescence to limit cycle. The induced PVC motion also became less energetic as the system makes this transition. Notably, a streak-like POD mode, resembling the center mode in the non-reacting case, dominates the transition case to limit-cycle oscillation. The DMD analysis extracts the same streak-like mode, supporting that the streak-like coherent structure arises from the center mode. The present research implies that the PVC may not be the only flow coherent structure that the flame interacts with during the onset of thermoacoustic oscillation. Marginally stable modes, such as the center mode, can be important in triggering thermoacoustic oscillation. Future work will continue to focus on the interaction between the flame and the center mode, as well as the dominance of such mode in the transitioning case.

Nomenclature

CH^*	CH* chemiluminescence intensity	U	time-averaged velocity
p	pressure	x	transverse coordinate
P	power	$\boldsymbol{x}$	spatial coordinate vector
$\boldsymbol{q}$	state vector of the flow field	y	vertical coordinate
r	radial coordinate	z	streamwise coordinate
R	radius of fused silica tube	θ	azimuthal coordinate
t	time	Φ	equivalence ratio
u	velocity	χ	molar fraction

Subscripts		Superscripts	
bulk	bulk flow	$\bar{}$	time averaged component
r	radial direction	$'$	fluctuation component
y	vertical direction	$\wedge$	mode shape
z	streamwise direction	$\sim$	nondimensional variable
th	thermal power		
θ	azimuthal direction		

References

[1] D. Dunn-Rankin, M. M. Miyasato, and T. K. Pham, *Lean Combustion*. Elsevier Inc., 2016.

[2] A. P. Dowling and A. S. Morgans, "Feedback Control of Combustion Oscillations," *Annu. Rev. Fluid Mech.*, no. 37, pp. 151–82, 2005.

[3] N. Syred, "A review of oscillation mechanisms and the role of the precessing vortex core (PVC) in swirl combustion systems," *Prog. Energy Combust. Sci.*, vol. 32, no. 2, pp. 93–161, Jan. 2006.

[4] K. Oberleithner, M. Stöhr, S. H. Im, C. M. Arndt, and A. M. Steinberg, "Formation and flame-induced suppression of the precessing vortex core in a swirl combustor_Experiments and linear stability analysis.pdf," *Combust. Flame*, vol. 162, pp. 3100–3114, 2015.

[5] S. Taamallah, S. J. Shanbhogue, and A. F. Ghoniem, "Turbulent flame stabilization modes in premixed swirl combustion : Physical mechanism and Karlovitz number-based criterion," *Combust. Flame*, vol. 166, pp. 19–33, 2016.

[6] Q. An and A. M. Steinberg, "The role of strain rate, local extinction, and hydrodynamic instability on transition between attached and lifted swirl flames," *Combust. Flame*, vol. 199, pp. 267–278, 2019.

[7] E. Karlis, Y. Liu, Y. Hardalupas, and A. M. K. P. Taylor, "Extinction strain rate suppression of the precessing vortex core in a swirl stabilised combustor and consequences for thermoacoustic oscillations," *Combust. Flame*, vol. 211, pp. 229–252,

2020.
[8] M. Stöhr, I. Boxx, C. D. Carter, and W. Meier, “Experimental study of vortex-flame interaction in a gas turbine model combustor,” *Combust. Flame*, vol. 159, pp. 2636–2649, 2012.
[9] S. Terhaar *et al.*, “Impact of Steam-Dilution on the Flame Shape and Coherent Structures in Swirl-Stabilized Combustors,” *Combust. Sci. Technol.*, vol. 186, pp. 889–911, 2014.
[10] Q. An, W. Y. Kwong, B. D. Geraedts, and A. M. Steinberg, “Coupled dynamics of lift-off and precessing vortex core formation in swirl flames,” *Combust. Flame*, vol. 168, pp. 228–239, 2016.
[11] K. T. Kim and S. Hochgreb, “Measurements of triggering and transient growth in a model lean-premixed gas turbine combustor,” *Combust. Flame*, vol. 159, no. 3, pp. 1215–1227, Mar. 2012.
[12] R. I. Sujith, M. P. Juniper, and P. J. Schmid, “Non-normality and nonlinearity in thermoacoustic instabilities,” *Int. J. Spray Combust. Dyn.*, vol. 8, no. 2, pp. 119–46, 2016.
[13] Z. Zhang, D. Zhao, S. H. Li, C. Z. Ji, X. Y. Li, and J. W. Li, “Transient energy growth of acoustic disturbances in triggering self-sustained thermoacoustic oscillations,” *Energy*, vol. 82, pp. 370–381, Mar. 2015.
[14] M. P. Juniper, “Triggering in the horizontal Rijke tube: Non-normality, transient growth and bypass transition,” *J. Fluid Mech.*, vol. 667, pp. 272–308, Jan. 2011.
[15] E. Karlis, “Transient and Limit Cycle Thermoacoustic Oscillation Dynamics in a Lean Premixed Swirl Stabilized Combustor,” Imperial College London, 2019.
[16] A. E. Bayley, Y. Hardalupas, and A. M. K. P. Taylor, “Local curvature measurements of a lean, partially premixed swirl-stabilised flame,” *Exp. Fluids*, vol. 52, no. 4, pp. 963–983, Apr. 2012.
[17] C. S. Panoutsos, Y. Hardalupas, and A. M. K. P. Taylor, “Effect of preheating on the local equivalence ratio at a swirl-stabilised partially-premixed combustor,” *46th AIAA Aerosp. Sci. Meet. Exhib.*, 2008.
[18] M. R. Khorrami, M. R. Malik, and R. L. Ash, “Application of Spectral Collocation Techniques to the Stability of Swirling Flows,” *J. Comput. Phys.*, vol. 81, pp. 206–29, 1989.
[19] S. Qiu, Z. Cheng, H. Xu, Y. Xiang, and H. Liu, “On the characteristics and mechanism of perturbation modes with asymptotic growth in trailing vortices,” *J. Fluid Mech.*, vol. 918, p. A41, Jul. 2021.
[20] L. Sirovich, “TURBULENCE AND THE DYNAMICS OF COHERENT STRUCTURES PART I : COHERENT STRUCTURES,” *Q. Appl. Math.*, vol. 45, no. 3, pp. 561–571, 1987.
[21] P.J.Schmid, “Dynamic mode decomposition of numerical and experimental data,” *J. Fluid Mech.*, vol. 656, pp. 5–28, 2010.
[22] Kutz JN, Brunton SL, Brunton BW, and Proctor JL, *Dynamic mode decomposition: data-driven modeling of complex systems.* 2016.
[23] M. P. Escudier, J. Bornstein, and T. Maxworthy, “The dynamics of confined vortices,” *Proc.R.Soc.Lond*, vol. 360, pp. 335–360, 1982.
[24] V. Theofilis, “Advances in global linear instability analysis of nonparallel and three-dimensional flows,” *Prog. Aerosp. Sci.*, vol. 39, pp. 249–315, 2003.
[25] A. Hagiwara and S. Bortz, “Studies on the near field aerodynamics of swirl burners,” International Flame Research Foundation, 1984.
[26] E. Karlis, Y. Liu, Y. Hardalupas, and A. M. K. P. Taylor, “H2 enrichment of CH4 blends in lean premixed gas turbine combustion : An experimental study on effects on flame shape and thermoacoustic oscillation dynamics,” *Fuel*, vol. 254, no. May, p. 115524,

2019.